Electrical Diagnosis Technique Using Differential Power Processing Converters for Photovoltaic Panels

Kazuma Honda
Department of Electrical and Electronic Engineering
Ibaraki University
Ibaraki, Japan
19nm657y@vc.ibaraki.ac.jp

Keito Aikawa
Department of Electrical and Electronic Engineering
Ibaraki University
Ibaraki, Japan
18nm601f@vc.ibaraki.ac.jp

Masatoshi Uno
Department of Electrical and Electronic Engineering
Ibaraki University
Ibaraki, Japan
masatoshi.uno.ee@vc.ibaraki.ac.jp

***Abstract*—Partial shading on a photovoltaic (PV) panel is well known to trigger not only significantly reduced power generation but also the occurrence of multiple maximum power points (MPPs). Various kinds of differential power processing (DPP) converters have been proposed and developed to address partial shading issues. Meanwhile, power generation of PV panels substantially decreases as panels deteriorate due to damage, and therefore, PV panels are desirably diagnosed for early detection of degradation and malfunctions. In recent years, autonomous electrical diagnosis techniques based on ac impedance measurement are considered as a promising solution, but conventional electrical diagnosis techniques require expensive instruments. This paper proposes a DPP converter as well as an electrical diagnosis technique using the DPP converter. The proposed DPP converter not only preclude the partial shading issues but also offer the electrical diagnosis capability based on ac impedance measurement. The operation analysis and experimental verification tests using a prototype of the proposed DPP converter were performed. The results demonstrated the improved power yield from partially shaded PV panels and the electrical diagnosis capability of the proposed DPP converter.**

Keywords*— *Photovoltaic Panel, Partial Shading, Differential Power Processing Converter, AC impedance measurement

I. Introduction

Renewable energy sources have gained attention, and photovoltaic (PV) panels have been installed in various application, such as residential rooftops, plug-in hybrid electric vehicles, and solar power plants. Partial shading on PV panels comprising multiple substrings connected in series is well known to trigger significantly reduced power generation. In the example case shown in Fig. 1(a), a shaded substring PV_3 that is less capable of generating current is bypassed by a bypass diode connected in parallel. The bypassed substring no longer contributes to power generation, and an extractable maximum power of the panel as a whole significantly decreases. For instance, 10% equivalent area of partial shading on a PV panel reportedly results in 30% reduction in annual energy yield [1]. In addition, multiple maximum power points (MPPs), including a global MPP and local MPP(s), appear on a *P–V* characteristic of partially-shaded panels and likely confuses ordinary MPP tracking algorithms.

To cope with partial shading issues, a variety of solutions to partial shading have been proposed and developed, as shown in Fig. 2. Distributed MPPT systems using micro-converters, also

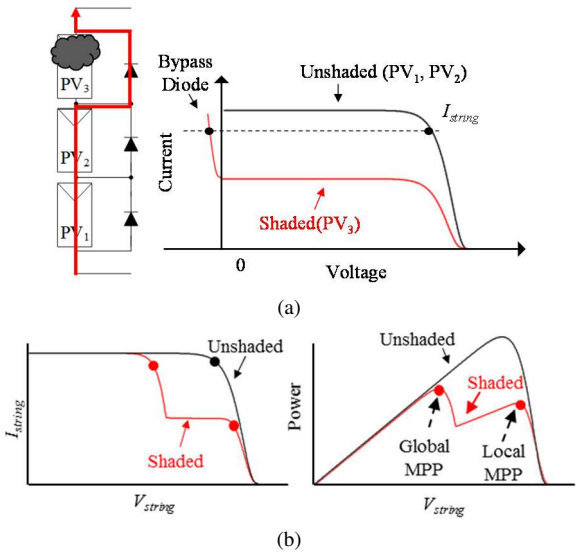

Fig. 1. Characteristics of (a) substrings and (b) panel under partial shading condition.

known as dc optimizers, have been employed to address issues, as shown in Fig. 2(a) [2]. With the micro-converters, all PV substrings can operate at each MPP, regardless of characteristic mismatch. However, since as many converters as the number of substrings are required, the complexity and cost of the system tend to soar.

Various kinds of differential power processing (DPP) converters or voltage equalizers have been proposed and developed to address partial shading issues [3]–[19]. The DPP converters transfer a fraction of the generated power of unshaded PV substrings to shaded ones so that all substrings characteristics are virtually unified, thus the partial shading issues are precluded. Since the DPP converters deal with only differential power between unshaded and shaded substrings, overall system efficiency can be improved compared to conventional systems using full power processing converters.

The DPP converters [3]–[19] are categorized in the architectures shown in Figs. 2(b) and (c). The adjacent substring-to-substring DPP converters, such as PWM converters [3]–[6], and switched capacitor converters [7]–[11], are employed in the architecture shown in Fig. 2(b). These DPP converters transfer power only between adjacent substrings, and therefore, power

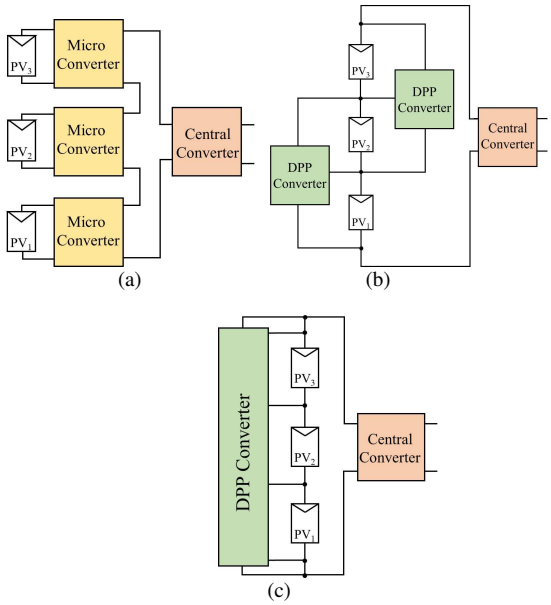

Fig. 2. Solutions to partial shading issues: (a) Distributed MPPT system using micro-converters, (b) adjacent substring-to-substring DPP converters, (c) string-to-substring DPP converter.

may have to traverse several DPP converters and substrings before reaching shaded substrings. Hence, the total power conversion efficiency is worsened due to collective power conversion loss. In addition, the numbers of DPP converters as well as switches are proportional to the number of substrings connected in series, likely increasing the system complexity and cost. The string-to-module DPP converter, such as the multi-winding flyback converter [12], LLC resonant voltage multipliers [13]–[17], and multi-stacked buck-boost converters [18], [19], are categorized in the architecture shown in Fig. 2(c). These DPP converters can dramatically reduce the converter count in comparison with other architectures. In other words, this architecture potentially achieves reduced cost, simplified circuit, and improved efficiency compared with the adjacent substring-to-substring DPP converter architecture.

Meanwhile, power generation of a PV system as a whole substantially decreases when a panel deteriorates due to damages and uneven aging. In order to operate the system efficiently, PV panels should be diagnosed to detect degradation and malfunctions as early as possible. Conventional diagnosis techniques using an *I–V* curve tracer or thermal camera, however, incur high costs due to maintenance personnel and expensive instruments. In recent years, an electrical diagnosis technique capable of an autonomous diagnosis based on ac impedance measurement is considered as a promising solution. Conventional ac impedance measurement techniques, however, also require expensive measurement instruments.

This paper proposes a string-to-substring DPP converter to address partial shading issues and an electrical diagnosis technique using the proposed DPP converter. The proposed DPP converter can not only preclude the partial shading issues but also offer the electrical diagnosis technique capability.

The rest of this paper is organized as follows. Section II introduces the proposed DPP converter and its electrical diagnosis technique. Section III presents the operation analysis for the proposed converter. The experimental results of a 24 W prototype for three substrings are shown in Section IV.

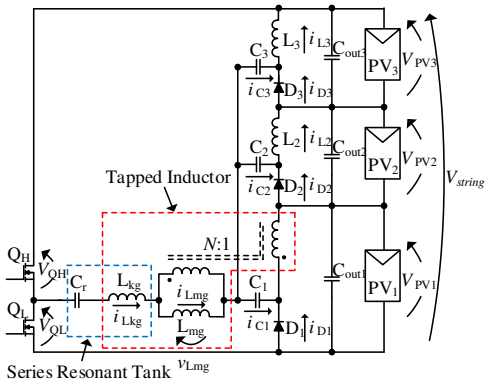

Fig. 3. Proposed DPP converter for three substrings.

II. Proposed DPP Converter

A. Topology

The proposed DPP converter for three substrings (PV_1–PV_3) connected in series is shown in Fig. 3. Substrings are connected to inductors L_2, L_3, and the secondary winding of the tapped inductor (TI). The series resonant tank consists of the leakage inductance of the TI, L_{kg}, and resonant capacitor C_r.

B. Features

Under partial shading conditions, equalization currents from the proposed DPP converter are supplied to shaded substrings to unify substring characteristics. Meanwhile, equalization currents need to be sinusoidally perturbated by adjusting the duty ratio for an electrical diagnosis using the proposed DPP converter. Although conventional string-to-substring DPP converters [12]–[17] are topologically simple, their equalization currents cannot be controlled nor adjusted by duty cycle. The proposed DPP converter, on the other hand, can perturb equalization currents by PWM control thanks to the inductors connected to each substring.

Conventional adjacent substring-to-substring DPP converters, such as PWM converters [3]–[6] and switched capacitor converters [7]–[11], require numerous switches in proportion to the number of substrings, whereas only two switches are necessary for the proposed DPP converter. Hence, the proposed DPP converter can simplify the circuit by reducing the switch count in comparison with the conventional adjacent substring-to-substring DPP converters.

C. AC Impedance Measurement Using DPP Converter

In general, an equivalent circuit of a PV substring consists of series resistance R_s, parallel resistance R_p, diffusion capacitance C_d, diode D, and constant current source, as shown in Fig. 4(a). Since the parameters of these passive elements are known to vary depending on degradation and irradiance [20], [21], panels can be diagnosed on the basis of parameter changes.

The Nyquist plot of a PV substring can be obtained by measuring an ac impedance *Z*, as shown in Fig. 4(b). The

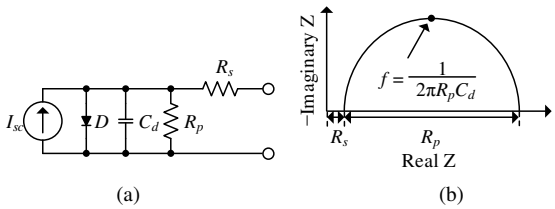

Fig. 4. (a) An equivalent circuit and (b) typical Nyquist plot of a PV substring.

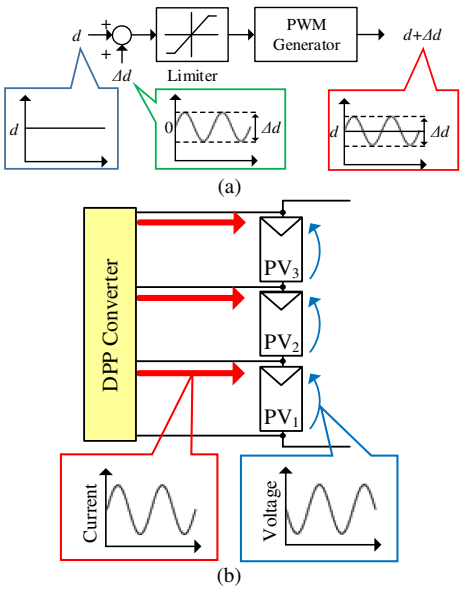

Fig. 5. (a) Control block diagram and (b) notional ac impedance measurement using DPP converter.

horizontal intercept of the semi-circle represents R_s, and the diameter of the semi-circle correspond to R_p. C_d is calculated from R_p and a frequency at the vertex.

A control block diagram and notional ac impedance measurement using the proposed DPP converter are illustrated in Figs. 5(a) and (b), respectively. For electrical diagnosis using the DPP converter, the duty cycle of Q_H, d, is sinusoidally perturbated so that Δd is superimposed on d in order to excite ac currents to each substring. Z is determined from the voltage responses to the supplied ac currents to the substrings.

III. Operation Analysis

A. Operation Principle

The key operation waveforms and current flow directions in the case that PV_1 is partially shaded are shown in Figs. 6 and 7, respectively.

Mode 1 ($t_0 \le t < t_1$) [Fig. 7(a)]: Q_H is turned on. The current of the resonant tank, i_{Lkg}, linearly increases and flows through the magnetizing inductor L_{mg} of the TI. i_{Lkg} is expressed as

$$i_{Lkg}(t) = \frac{\left(N + \frac{1}{N}\right)\left(\frac{V_{string}}{N+1} - V_{PV}\right)}{L_{mg}}(t - t_0) + i_{Lkg}(t_0) \tag{1}$$

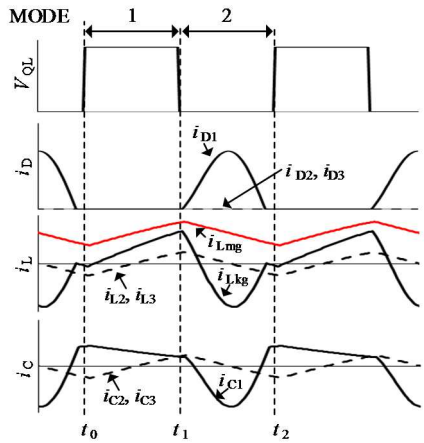

Fig. 6. Key operation waveforms when PV_1 is partially shaded.

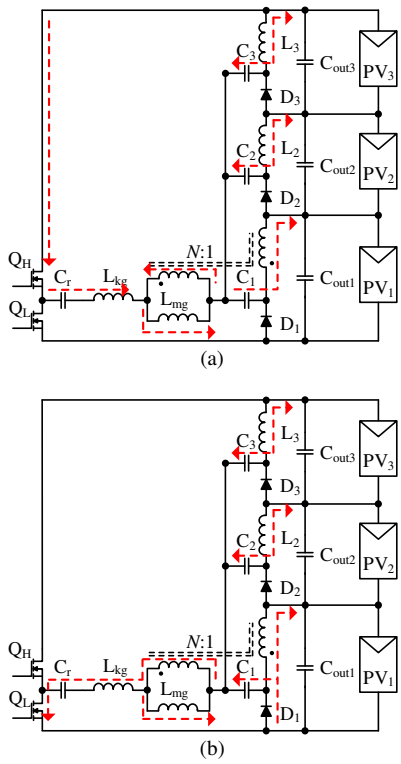

Fig. 7. Current flow directions when PV_1 is shaded: Modes (a) 1 and (b) 2.

where N is the turn ratio of the TI, V_{PV} and V_{string} are the substring and panel voltages, respectively.

The average voltage at the switching node is equal to dV_{string}. Meanwhile, the average voltage at the cathode pin of D_1 is V_{PV}. Hence, the sum of the average voltages of C_1 and C_r is $dV_{string} - V_{PV}$. The voltage applied to L_{mg}, v_{Lmg}, is

$$\begin{aligned} v_{Lmg} &= \frac{N}{N+1}\left\{\left(V_{string} - V_{PV}\right) - \left(dV_{string} - V_{PV}\right)\right\} \\ &= \frac{N}{N+1}(1-d)V_{string} \end{aligned} \tag{2}$$

Mode 2 ($t_1 \le t < t_2$) [Fig. 7(b)]: Q_L is turned on. The leakage inductor L_{kg} and the resonant capacitor C_r resonate, and i_{lkg} sinusoidally flows through D_1 and C_1. i_{lkg} is expressed as

$$i_{Lkg}(t) = \frac{-NV_{PV}}{|Z_r|} e^{-\gamma(t-t_1)} \sin\omega_r(t-t_1) + i_{Lkg}(t_1) \quad (3)$$

where Z_r is the characteristic impedance of the resonant tank, γ is damping factor, and ω_r is the damped resonant angular frequency. Z_r, γ, and ω_r are given by

$$Z_r = \sqrt{\frac{L_{kg}}{C_r}},\ \gamma = \frac{R}{2L_{kg}},\ \omega_r = \sqrt{\frac{1}{L_{kg}C_r} - \gamma^2} \quad (4)$$

where R is the total resistance of the resonant current paths.

Since the diode D_1 conducts, the voltages of L_2, L_3, and the secondary winding of the TI are connected to each substring in parallel. The voltages of inductors are determined to be V_{PV}, thus v_{Lmg} is expressed as

$$v_{Lmg} = -NV_{PV} \quad (5)$$

The diode D_1 conducts whereas other diodes are off. The shaded substring PV_1 receives the equalization current. After half the resonant period, no current flows through D_1. Since the average current of C_1 must be zero under steady-state conditions, the average current of D_1 and the secondary winding of the TI are equal to the equalization current I_{eq} for shaded substring PV_1. Under steady-state conditions, the primary winding of the TI is sandwiched between C_r and C_1–C_3, thus its average current is equal to I_{eq}/N. On the other hand, no current flows toward unshaded substrings, hence the average current of L_2 and L_3 are zero.

B. Voltage Conversion Ratio

All the substring voltages are assumed equal to V_{PV}. From the volt-sec balance on inductors, (2) and (5) yield

$$V_{PV} = \frac{d}{N+1} V_{string} \quad (6)$$

This equation suggests that the voltage of each substring can be regulated by PWM control manipulating d.

Since the DPP converter needs to be properly controlled so that no currents flow toward the unshaded substrings, ΔV-controlled strategy [22] is applied to the proposed DPP converter. With the ΔV-controlled strategy, the DPP converter operates to regulate the voltage difference $\Delta V = V_{Unshaded} - V_{Shaded}$ (where $V_{Unshaded}$ and V_{Shaded} are the unshaded and shaded substring voltages, respectively). The value of ΔV should be determined to fulfill the following equation;

$$\Delta V \geq I_{eq\_max} R_{eq} \quad (7)$$

where $I_{eq.max}$ and R_{eq} are the largest equalization current and the equivalent resistance of the DPP converter, respectively.

IV. Experimental Results

A. Prototype

A prototype of the proposed DPP converter that can supply 24 W for each shaded substring was built for three substrings connected in series, as shown in Fig. 8. Component values are listed in Table I. The prototype was operated at 100 kHz.

B. Measured Waveforms and Power Conversion Efficiency

The experimental setup shown in Fig. 9 was used to measure the power conversion efficiency of the prototype. Substrings PV_1–PV_3 were removed, and a variable resistor R_{var} was connected to C_{out1} to emulate the current flow paths under the PV_1-shaded condition. I_{Rver} demonstrates the equalization current I_{eq}. The prototype was operated with $d = 0.5$ and a fixed input voltage of $V_{in} = 36$ V, which was equivalent to the MPP voltage of a panel.

Measured key waveforms at $I_{Rvar} = 2.0$ A are shown in Fig. 10. These waveforms were in good agreement with the theoretical ones shown in Fig. 6. The measured power conversion efficiency and output characteristics are shown in Fig. 11. From the measured output I–V characteristic, the value of R_{eq} was calculated to be 0.45 Ω. The measured peak efficiency was as high as 92.6%. In the light load region lower than 7.8 W, the most dominant loss factor was considered to be the diode conduction losses. On the other hand, the copper loss of the TI and conduction loss of the switches were dominant losses in the heavy load region higher than 15 W.

C. Experimental Equalization Test Emulating Partial Shading Condition

An experimental equalization test using solar array simulators (E4361A, Keysight Technologies) was performed

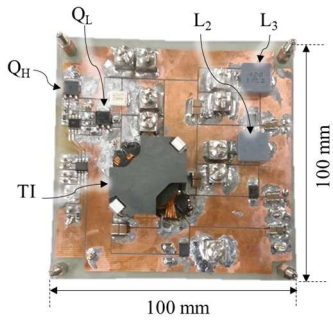

Fig. 8. Photograph of the proposed DPP converter for three substrings.

TABLE I. Component Values

Component	Values
Q_H, Q_L	FDD390N15A, R_{on} = 33.5 mΩ
C_1–C_3	Ceramic Capacitor, 44 μF
C_{out1}–C_{out3}	Ceramic Capacitor, 200 μF
C_r	Film Capacitor, 470 nF
D_1–D_3	Schottky Diode, V_f = 0.43 V
Tapped Inductor	N_1:N_2 = 10:20, L_{kg} = 1.0 μH, L_{mg} = 52 μH
L_2, L_3	47 μH

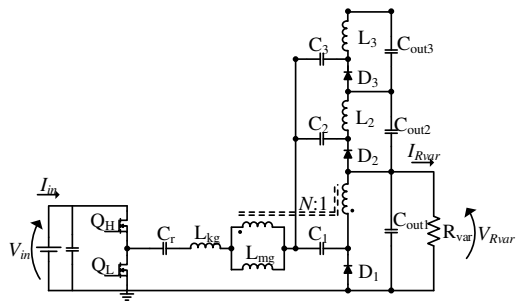

Fig. 9. Experimental setup for efficincy measurement.

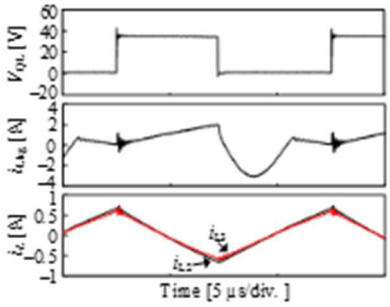

Fig. 10. Measured key waveforms when PV_1 is partially shaded.

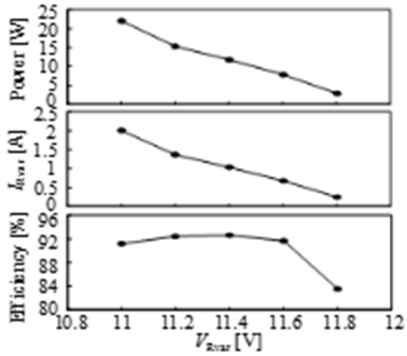

Fig. 11. Measured power conversion efficiency and output current characteristic.

emulating PV_1-shaded condition. Individual substring characteristics used for the experiment are shown in Fig. 12(a), and the mismatch in short-circuit current was approximately 1.5 A. The theoretical extractable maximum power was 146 W if all substrings could ideally operate at each MPP. The panel characteristics were manually swept using an electronic load. Based on (7), ΔV was determined to be 700 mV (≈ 1.5 A × 0.45 Ω) by assuming $I_{eq.max}$ = 1.5 A.

The measured panel characteristics with/without the DPP converter are compared in Fig. 12(b). Without the proposed DPP converter, two MPPs were observed, and the maximum power was 122 W. With the proposed DPP converter, the local MPP disappeared, and the maximum power increased to as high as 142 W, corresponding to 16.4% improvement and the overall efficiency of 97.3% (= 142/146 W). The experimental result demonstrated the enhanced energy yield by the proposed DPP converter.

D. Experimental AC Impedance Measurement Using PV Substring Emulators

To facilitate the experiment in the laboratory, PV substring emulators based on the equivalent circuit shown in Fig. 4(a) were prepared. As shown in Fig. 13(a), the PV substring emulator consists of series and parallel resistance, capacitor, diode, and a current source composed of an isolated dc-dc converter and a linear regulator. I–V characteristics of the PV substring emulators used for the experiment are shown in Fig. 13(b).

The experimental setup to measure ac impedance using the proposed DPP converter is depicted in Fig. 14. The currents and

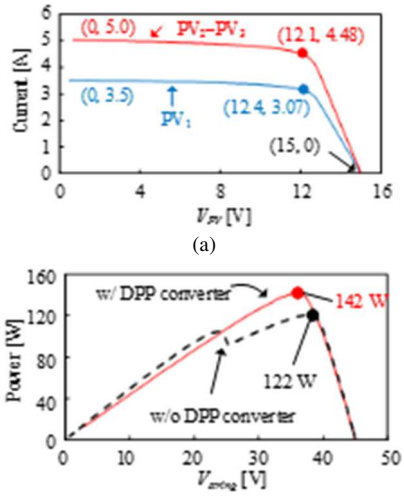

(a)

(b)

Fig. 12. Experimental results of the equalization test: (a) Individual PV substring charactristics. (b) Panel characteristics with/without DPP converter.

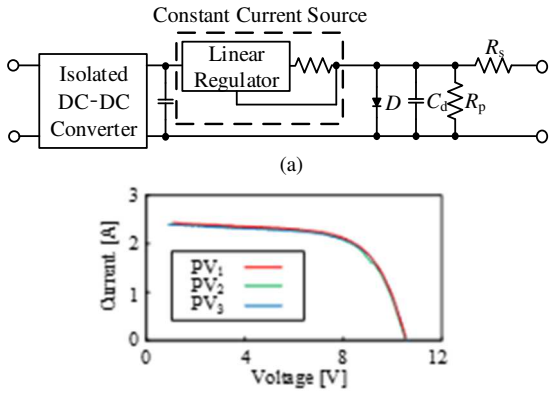

(a)

(b)

Fig. 13. (a) PV substring emulator and (b) its I–V characteristic.

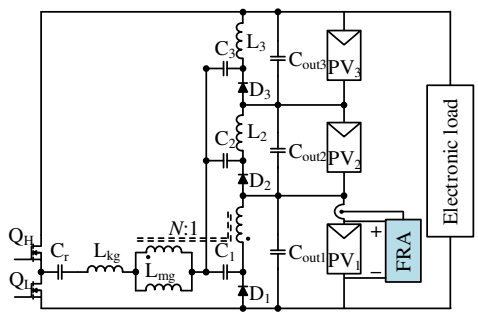

Fig. 14. Experimental setup for ac impedance measurement.

voltages of the substring emulators were measured using the frequency response analyzer (FRA). The prototype was operated with d = 0.5 and Δd = 0.1. The values of R_s, R_p, and C_d were also measured using the FRA alone to compare with the proposed DPP converter.

The Nyquist plots measured by the FRA alone or by the proposed DPP converter are compared in Fig. 15. Parameters of the passive elements were calculated from the measured Nyquist

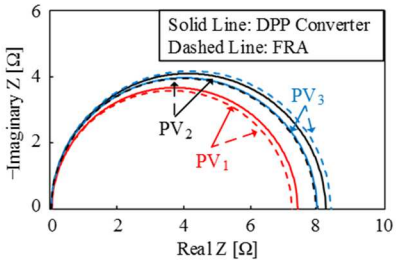

Fig. 15. Measured Nyquit plots with FRA/DPP converter.

TABLE II. CALCULATED PARAMETERS OF PSSIVE ELEMENTS

Element	FRA	DPP converet	Error
R_s	55.5 mΩ	58.4 mΩ	5.27%
R_p	7.16 Ω	7.34 Ω	2.48%
C_d	172 μF	180 μF	5.05%

plots, as shown in Table II. The calculated parameters by the proposed DPP converter were in good agreement with those measured by the FRA alone, corresponding to errors less than 5.27%. The result demonstrated the efficacy of the proposed electrical diagnosis technique.

V. CONCLUSION

The DPP converter and its electrical diagnosis technique for PV panels have been proposed in this paper. The proposed DPP converter not only precludes the partial shading issues but also offers the electrical diagnosis capability based on the ac impedance measurement.

The experimental equalization test using the prototype of the proposed DPP converter for three substrings connected in series was performed emulating the partial shading condition. With the proposed DPP converter, a local MPP successfully disappeared, and the extractable maximum power increased. In addition, the experimental ac impedance measurement using the PV substring emulators was also performed with the proposed DPP converter. The calculated parameters using the proposed DPP converter agreed well with those measured by the FRA alone. The result demonstrated the electrical diagnosis capability of the proposed DPP converter.

REFERENCES

[1] S. M. MacAlpine, R. W. Erickson, and M. J. Brandemuehl, "Characterization of power optimizer potential to increase energy capture in photovoltaic systems operating under nonuniform conditions," *IEEE Trans. Power Electron*., vol. 28, no. 6, pp. 2936–2945, Jun. 2013.

[2] S. Poshtkouhi, V. Palaniappan, M. Fard, and O. Trescases, "A general approach for quantifying the benefit of distributed power electronics for fine grained MPPT in photovoltaic applications using 3-D modeling," *IEEE Trans. Power Electron*., vol. 27, no. 11, pp. 4656–4666, Nov. 2012.

[3] T. Shimizu, M. Hirakata, T. Kamezawa, and H. Watanabe, "Generation control circuit for photovoltaic modules," *IEEE Trans. Power Electron*., vol. 16, no. 3, pp. 293–300, May 2001.

[4] P. S. Shenoy, K. A. Kim, B. B. Johnson, and P. T. Krein, "Differential power processing for increased energy production and reliability of photovoltaic systems," *IEEE Trans. Ind. Power Electron.*, vol. 28, no. 6, pp. 2968–2979, Jun. 2013.

[5] H. J. Bergveld, D. Büthker, C. Castello, T. Doorn, A. D. Jong, R. V. Otten, and K. D. Waal, "Module-level DC/DC conversion for photovoltaic systems: the delta-conversion concept," *IEEE Trans. Power. Electron*., vol. 28, no. 4, pp. 2005–2013, Apr. 2013.

[6] S. Qin and R. C. N. P. Podgurski, "Sub-module differential power processing for photovoltaic applications," in Proc. *IEEE. Applied Power Electron. Conf.* Expo., pp. 101–108, 2013.

[7] A. H. Chang, A. T. Avestruz, and S. B. Leeb, "Capacitor-less photovoltaic cell-level power balancing using diffusion charge redistribution," *IEEE Trans. Power. Electron*., vol. 30, no. 2, pp. 537–546, Feb. 2015.

[8] M. Uno, Y. Saito, M. Yamamoto, and S. Urabe, "PWM switched capacitor-based cell-level power balancing converter utilizing diffusion capacitance of photovoltaic cells," *IEEE Trans. Power Electron*., to be published.

[9] M. Uno, M. Yamamoto, H. Sato, and S. Oyama, "Modularized differential power processing architecture based on switched capacitor converter to virtually unify mismatched photovoltaic panel characteristics," *IEEE Trans. Power Electron*., to be published.

[10] M. Uno and A. Kukita, "PWM converter integrating switched capacitor converter and series-resonant voltage multiplier as equalizers for photovoltaic modules and series-connected energy storage cells for exploration rovers," *IEEE Trans. Power. Electron*., vol. 32, no. 11, pp. 8500–8513, Nov. 2017.

[11] M. Gokdaga, M. Akbabab, and O. Gulbudakc, "Switched-capacitor converter for PV modules under partial shading and mismatch conditions," *Solar Energy*, vol. 170, pp. 723–731, Aug. 2018.

[12] J. Du, R. Xu, X. Chen, Y. Li, and J. Wu, "A novel solar panel optimizer with self-compensation for partial shadow condition," in Proc. *IEEE Applied Power Electron. Conf. Expo*., pp. 92–96, 2013.

[13] M. Uno and A. Kukita, "Two-switch voltage equalizer using an LLC resonant inverter and voltage multiplier for partially-shaded series-connected photovoltaic modules," *IEEE Trans. Ind. Appl*., vol. 51, no. 2, pp. 1587–1601, Mar/Apr. 2015.

[14] M. Uno and A. Kukita, "Single-switch single-magnetic PWM converter integrating voltage equalizer for partially-shaded photovoltaic modules in standalone applications," *IEEE Trans. Power Electron*., vol. 33, no. 2, pp. 1259–1270, Feb. 2018.

[15] M. Uno and T. Shinohara, "Variable switching frequency modulation scheme for PWM converter integrating series-resonant voltage multiplier-based voltage equalizer for photovoltaic strings under partial shading," *IEEJ Trans. Electrical Electronics Engineering*., vol. 14, no. 3, pp. 467–474, Mar. 2019.

[16] M. Uno, T. Shinohara, Y. Saito, and A. Kukita, "Review, comparison, and proposal for PWM converters integrating differential power processing converter for small exploration rovers," *Energies*, pp. 1–19, May 2019.

[17] M. Uno and T. Shinohara, "Module-integrated converter based on cascaded quasi-Z-source inverter with differential power processing capability for photovoltaic panels under partial shading," *IEEE Trans. Power Electron*., to be published.

[18] M. Uno and A. Kukita, "Single-switch voltage equalizer using multi-stacked buck-boost converters for partially-shaded photovoltaic modules," *IEEE Trans. Power Electron*., vol. 30, no. 6, pp. 3091–3105, Jun. 2015.

[19] M. Uno and A. Kukita, "Current sensorless equalization strategy for a single-switch voltage equalizer using multistacked buck–boost converters for photovoltaic modules under partial shading," *IEEE Trans. Ind. Appl*., vol. 53, no. 1, pp. 420–429, Jan/Feb. 2017.

[20] M. Sugiyama, M. Hayashi, C. Yamazaki, N.B. Hamidon, Y. Hirose, and M. Itagaki, "Application of impedance spectroscopy to investigate the electrical properties around the pn interface of Cu(In,Ga)Se_2 solar cells," *Thin Solid Film*, vol. 535, pp. 287–290, May 2013.

[21] M. Sugiyama, H. Sakakura, S.W. Chang, M. Itagaki, "Investigation of sputtering damage around pn interfaces of Cu(In,Ga)Se_2 solar cells by impedance spectroscopy," *Electrochimica Acta*, vol. 131, pp. 236–239, Jun. 2014.